



Prussian blue nanocubes on nitrobenzene-functionalized reduced graphene oxide and its application for H₂O₂ biosensing



Li Wang ^{a,*}, Yinjian Ye ^a, Xingping Lu ^a, Yi Wu ^a, Lanlan Sun ^b, Hongliang Tan ^a, Fugang Xu ^a, Yonghai Song ^a

^a College of Chemistry and Chemical Engineering, Jiangxi Normal University, 99 Ziyang Road, Nanchang 330022, People's Republic of China

^b State Key Laboratory of Luminescence and Applications, Changchun Institute of Optics, Fine Mechanics and Physics, Chinese Academy of Sciences, 3888 East Nan-Hu Road, Changchun 130033, People's Republic of China

ARTICLE INFO

Article history:

Received 17 June 2013

Received in revised form 9 October 2013

Accepted 10 October 2013

Available online 23 October 2013

Keywords:

Biosensor

Prussian blue nanocubes

Reduced graphene oxide

Nitrobenzene

H₂O₂

ABSTRACT

Detection of H₂O₂ is very important in biological analysis, clinical diagnosis, food industry, etc. This work presents an electrochemical approach for the detection of H₂O₂ based on Prussian blue (PB) nanocubes-nitrobenzene-reduced graphene oxide (RGO) nanocomposites (PB nanocubes-nitrobenzene-RGO). The hybrid nanocomposites were constructed by growing PB nanocubes onto the nitrobenzene-RGO composites which were prepared by spontaneous grafting nitrophenyl groups to the basal carbon atoms of RGO based on chemical bonding. The obtained PB nanocubes-nitrobenzene-RGO nanocomposites were characterized by scanning electron microscopy, X-ray diffraction and Fourier transform infrared spectroscopy. The formation mechanism of PB nanocubes-nitrobenzene-RGO nanocomposites was investigated and discussed in detail. The PB nanocubes-nitrobenzene-RGO modified glassy carbon electrode shows good electrocatalysis toward the reduction of H₂O₂. The resulted H₂O₂ biosensor exhibited a rapid response of 2 s, a low detection limit of 0.4 μM, a wide linear range of 1.2 μM to 15.25 mM and high sensitivity of 300.16 μA cm⁻² mM⁻¹, as well as good stability, repeatability and selectivity. Further immobilizing glucose oxidase on the PB nanocubes-nitrobenzene-RGO nanocomposites/GCE, an amperometric glucose biosensor was achieved by monitoring the generated H₂O₂ under a relatively negative potential. The sensors might be used as a promising one for practical application.

© 2013 Elsevier Ltd. All rights reserved.

1. Introduction

Hydrogen peroxide (H₂O₂), as an important chemical, is widely used in food, pharmaceutical, chemical and biochemical industries [1]. H₂O₂ is not only a by-product of several highly selective oxidases, but also an essential mediator in biology, medicine, industry and many other fields [2]. Therefore, the accurate determination of H₂O₂ has become extremely important in recent years.

To date, various techniques have been developed for H₂O₂ determination, including titrimetry [3], spectrofluorometry [4], spectrophotometry [5,6], chemiluminescence [7] and electrochemistry [8–10], etc. Among those techniques, the electrochemistry has attracted significant attention because of its high sensitivity, low cost, simplicity and rapid response [10–12]. The electrochemical approach for H₂O₂ detection can be realized by using peroxidase or protein (such as horseradish peroxidase, cytochrome c) as recognition element to monitor the current change in the process of the oxidation or reduction of H₂O₂ catalyzed by peroxidase or protein [13–16]. Despite the low detection limit and

high selectivity, the use of the peroxidase or protein obviously deteriorates transducer properties due to its poor direct electrochemistry. Furthermore, peroxidase or protein-based sensor involves complicated, multi-step immobilization procedures [17]. Under critical operating conditions, the measurements suffer from poor reproducibility, thermal and chemical instability and high cost [18]. Environmental conditions such as temperature, pH, and humidity and the presence of ionic detergents and enzyme-poisoning molecules in the sample can easily interrupt the performance of sensors [18].

A method to overcome the disadvantages of protein-based biosensor is developing nanomaterials with peroxidase-like activity. Nanoscaled Fe₃O₄ was firstly reported to possess intrinsic peroxidase-like activity [19] and to be used as recognition element for the determination of H₂O₂ [20,21]. Many nanomaterials, including Au [22], Ag [23–25], Pd [26], Pt [27–29], CuO [30], etc., have been also used to construct electrochemical H₂O₂ sensors. Prussian blue (PB), as a prototype of metal hexacyanoferrate with the formula of Fe^{III}₄[Fe^{II}(CN)₆]₃, has been widely used as the electron-transfer mediator in the electrochemical H₂O₂ sensor because it can catalyze the electrochemical reduction of H₂O₂ at low overpotentials (it is usually referred to artificial enzyme peroxidase) [31–35]. To realize the application, high-quality active

* Corresponding author. Tel.: +86 791 88120861; fax: +86 791 88120861.

E-mail address: lwangs@jxnu.edu.cn (L. Wang).

supports are usually required for the immobilization of PB to improve the sensor's stability and sensitivity. Graphene or reduced graphene oxide (RGO) is a new type of two-dimensional carbon nanostructure with a single layer of carbon atoms densely packed in a honeycomb lattice [36]. It has unique conductivity, mechanical properties and high specific surface area owing to long-range π -conjugation [37,38] and was extensively used in electrochemical sensor [39]. These special characteristics prompt the application of graphene or RGO as a support to synthesize hybrid PB-graphene (or RGO) nanocomposites for electrochemical H₂O₂ sensor [31–33,35,40,41]. To load a large number of PB, graphene was usually transformed into graphene oxide (GO) (a small number of carboxyl group on GO) or functionalized by some molecules based on physical absorption [32,40]. However, the poor immobilization usually resulted in falling off PB from the nanosheet during electrochemical analysis or under agitation and stirring. Consequently, thus prepared sensor suffers from poor reproducibility, thermal, mechanical and chemical instability, regardless of high sensitivity and low detection limit. Therefore, more efforts are still needed to design novel PB-graphene (or RGO) nanocomposites for developing reliable electrochemical H₂O₂ sensor.

In this work, RGO was firstly functionalized by spontaneous grafting nitrophenyl groups to the basal carbon atom of RGO based on chemical bonding. Then, PB nanocubes-nitrobenzene-RGO nanocomposites were constructed by controllable growth of PB nanocubes monolayers on nitrobenzene-RGO composites. The formation mechanism of the nanocomposites was discussed. The PB nanocubes-nitrobenzene-RGO nanocomposites show good stability under critical operating conditions and a reliable H₂O₂ biosensor was developed by immobilizing the PB nanocubes-nitrobenzene-RGO nanocomposites on glassy carbon electrode (GCE). The experimental conditions related to the preparation of PB nanocubes-nitrobenzene-RGO nanocomposites and the performances of the resulted sensor were investigated in detail.

2. Experimental

2.1. Reagents and materials

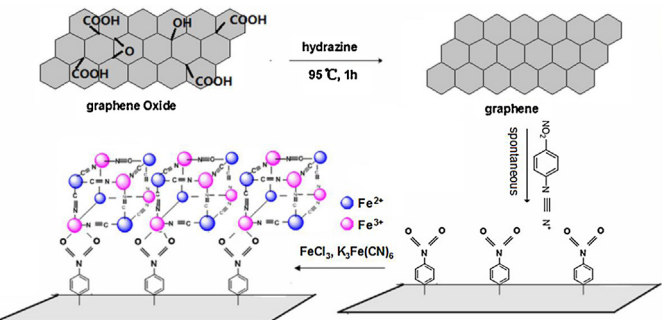
Graphite powder (spectrum pure), potassium ferricyanide ($K_3Fe(CN)_6$), potassium chloride (KCl), ferric chloride ($FeCl_3 \cdot 6H_2O$), chitosan (CHIT, 75% deacetylation), hydrogen peroxide (H_2O_2) solution (30 wt%) and other chemicals were obtained from Shanghai Chemical Reagent Co. (Shanghai, China). Glucose oxidase (GOD, EC1.1.3.4, Type X-S, lyophilized powder, 117 U mg⁻¹, from Aspergillusniger), D-(+)-glucose ($\geq 99.5\%$), nitrophenyl diazonium tetrafluoroborate and tetrabutylammonium were obtained from Sigma-Aldrich (St. Louis, USA). All the chemicals in this work were of analytical grade. Phosphate buffer solutions (PBS, 0.05 M, pH 6.0) were prepared with KH_2PO_4 and K_2HPO_4 , containing 0.1 M KCl. All solutions were prepared with ultra-pure water purified by a Millipore-Q System (18.2 MΩ cm).

2.2. Synthesis of GO and RGO

GO was synthesized according to previous methods [42]. The RGO was prepared by reduction of GO with hydrazine. Typically, hydrazine (0.12 mL) was added into the dispersion of GO (100 mg GO in 100 mL water) and sonicated for 1 h. Then the mixture was reacted at 90 °C under constant stirring for 1 h. RGO was obtained by filtering the product and drying in vacuum.

2.3. Synthesis of nitrobenzene-RGO composites

The nitrobenzene-RGO composites were prepared by spontaneous grafting nitrophenyl groups to the basal carbon atoms



Scheme 1. Procedure for the fabrication of PB nanocubes-nitrobenzene-RGO nanocomposites.

according to previous procedure [43]. Briefly, 12 mg RGO was dispersed in 10 mL degassed acetonitrile (ACN) by ultrasonication for about 1 h. Then 24 mg (10 mM) nitrophenyl diazonium tetrafluoroborate and 0.329 mg (0.1 M) tetrabutylammonium was added into above solution. After the mixture was placed in the absence of light for 5 h, it was washed with ACN and acetone and dried at 80 °C for 4 h. The preparation of nitrobenzene-RGO composites is illustrated in Scheme 1.

2.4. Synthesis of PB nanocubes-nitrobenzene-RGO nanocomposites

The PB nanocubes-nitrobenzene-RGO nanocomposites were prepared according to a previous procedure [44]. Briefly, 5 mg nitrobenzene-RGO composites were reacted with 10 mL $FeCl_3$ aqueous solution (pH = 1.0 adjusted with HCl) by ultrasonic agitation for 1 h. Then 10 mL aqueous solution of $K_3Fe(CN)_6$ (pH = 1.0) was added dropwise to this mixture with continuous stirring at room temperature. After that, the mixture was maintained at 90 °C for different reaction time to yield a suspension of PB nanocubes-nitrobenzene-RGO nanocomposites. The solid product was then centrifuged and washed with ultra-pure water for several times until no Cl^- was detected by $AgNO_3$. Finally, the product was dried at 80 °C for 4 h in an oven. The preparation of PB nanocubes-nitrobenzene-RGO nanocomposites is illustrated in Scheme 1.

2.5. Preparation of PB nanocubes-nitrobenzene-RGO nanocomposites/GCE

A glassy carbon electrode (GCE, 3 mm in diameter) was polished with 1.0, 0.3, 0.05 μ m alumina powder, respectively. Then the polished GCE was rinsed with ultra-pure water followed by sonicating in ultra-pure water for 1 min. A defined amount of PB nanocubes-nitrobenzene-RGO nanocomposites (1.0 mg) were suspended in 500 μ L ultra-pure water containing 5 μ L chitosan (0.5 wt%) and sonicated for 30 min. Then a drop of the suspension was cast on the polished GCE surface and dried in air. When the resulted PB nanocubes-nitrobenzene-RGO/GCE were not in use, it was stored in the inverted beaker at room temperature.

2.6. Preparation of GOD/PB nanocubes-nitrobenzene-RGO nanocomposites/GCE

5.0 μ L GOD and 3.0 μ L chitosan solutions (0.5 wt%) were mixed and dropped onto PB nanocubes-nitrobenzene-RGO nanocomposites/GCE, drying in air at 4 °C for 12 h to obtain a GOD/PB nanocubes-nitrobenzene-RGO nanocomposites/GCE. When the GOD/PB nanocubes-nitrobenzene-RGO nanocomposites/GCE was not in use, it was also stored in the inverted beaker at 4 °C.

2.7. Apparatus

All electrochemical experiments were performed by a CHI 660C electrochemical workstation (CH Instruments, Shanghai, China) using a conventional three-electrode system with a bare or modified GCE as the working electrode, a platinum wire as the auxiliary electrode, and a Ag/AgCl (saturated with KCl) as the reference electrode. The cyclic voltammetric experiments were performed in a quiescent solution. The amperometric experiments were carried out in a continuous stirring solution using a magnetic stirrer. Atomic force microscopy (AFM) measurements were carried out with an AJ-III (Shanghai Aijian Nanotechnology, China) using a tapping mode. Standard silicon cantilevers (spring constant 0.6–6 N m⁻¹) were used under their resonance frequency (typically, 60–150 kHz). All AFM images were acquired under the ambient conditions, and images were raw data except for flattening. X-ray powder diffraction (XRD) data were collected on a D/Max 2500 V/PC X-ray powder diffractometer using Cu K α radiation ($\lambda=1.54056\text{ \AA}$, 40 kV, 200 mA). The scanning electron microscopy (SEM) analysis was taken using a XL30 ESEM-FEG SEM at an accelerating voltage of 20 kV equipped with a Phoenix energy dispersive X-ray analyzer (EDXA). Fourier transform infrared spectroscopy (FTIR) was obtained on a Perkin-Elmer Spectrome 100 spectrometer (Perkin-Elmer Company, USA).

3. Results and discussion

3.1. Characteristics of nitrobenzene-RGO composites

The nitrobenzene-RGO composites were examined by FTIR (Fig. 1A). The spectrum of the nitrophenyl-functionalized RGO exhibits new bands at 1579 and 1346 cm⁻¹, which fall within the range of the symmetric and asymmetric stretching modes of the NO₂ group [43]. The bands located at 1218, 1124, and 1524 cm⁻¹ correspond to C–N stretching vibration, C–H bending, and C=C stretching vibration of benzene ring, respectively. Other bands located at 1386, 1636 and 1732 cm⁻¹ correspond to D band, C=C stretching vibration and C=O stretching vibration of RGO [45]. The result indicated that the nitrophenyl was grafted on RGO surface based on chemical bonding.

The nitrobenzene-RGO composites can be dispersed very well in water at the level of individual sheets. Fig. 1B shows the AFM image of nitrobenzene-RGO composites. Individual sheets with very smooth surface could be easily observed in this image, suggesting nitrophenyl was grafted on RGO surface to form well-ordered monolayers [43]. Section analysis showed that the thickness of nitrobenzene-RGO composite sheets was about 1.2 nm. Since the length of the nitrobenzene was about 0.5 nm [46] and the thickness of the RGO was about 0.5 nm [47], it was reasonable to conclude that the nitrobenzene-RGO composites consisted of one layer of RGO and monolayer of nitrobenzene attaching on both sides of RGO. When a nitrobenzene molecule was grafted onto the RGO surface parallel to the surface normal axis, the height of the layer should be 1.5 nm. However, the height of nitrobenzene-RGO composites was only 1.2 nm. Thus it suggested that the molecules could not stand fully perpendicular to the substrate, instead a 30° tilt in the molecular conformation of nitrobenzene on RGO surface may be adopted [48].

3.2. Controllable growth of PB nanocubes-nitrobenzene-RGO nanocomposites

After the nitrobenzene-RGO composites were immersed into the solution of Fe³⁺, the Fe³⁺ strongly interacted with nitro-groups and adsorbed on the nitro-groups based on the electrostatic

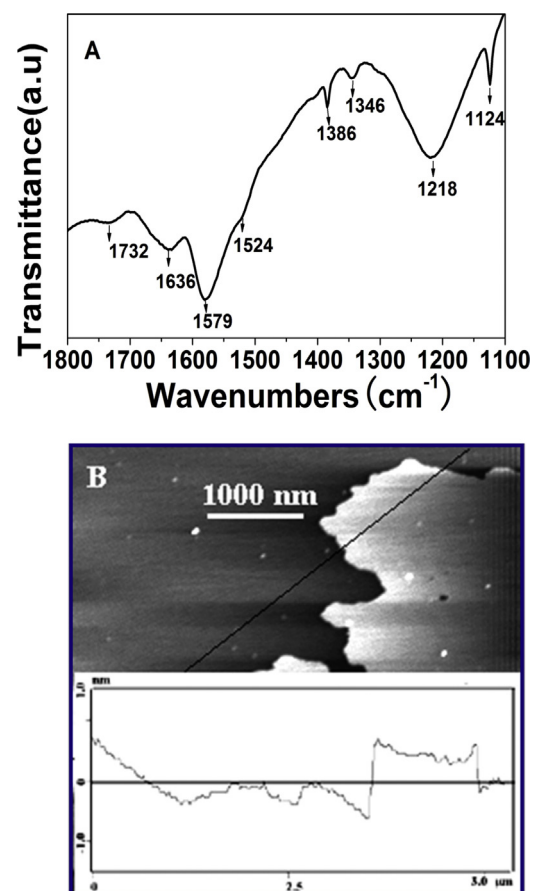


Fig. 1. (A) FTIR of nitrobenzene-RGO composites. (B) AFM image of nitrobenzene-RGO composites and the corresponding to height profile of the AFM image.

interactions and coordination interaction [32]. Then, the Fe(CN)₆³⁻ would coordinate with the Fe³⁺ on the surface of nitrobenzene-RGO composites and resulted in the formation of Fe^{III}–Fe^{III}(CN)₆³⁻ metal-organic frameworks [49,50]. Subsequently, the electron transfer from nitrobenzene-RGO composites to the absorbed Fe^{III}–Fe^{III}(CN)₆³⁻ metal-organic frameworks resulted in the formation of PB nanostructures [32,33,49,50]. The growth of PB nanostructures-nitrobenzene-RGO nanocomposites as a function of the concentration of FeCl₃–K₃Fe(CN)₆ was followed by SEM (Fig. 2). The SEM image of PB nanostructures-nitrobenzene-RGO nanocomposites obtained at 0.4 mM FeCl₃–K₃Fe(CN)₆ (Fig. 2A) shows a uniform surface topography, suggesting that small quantity of FeCl₃–K₃Fe(CN)₆ metal-organic frameworks on nitrobenzene-RGO composites is not enough to form detectable PB nanostructures. As the concentration of FeCl₃–K₃Fe(CN)₆ was increased to 0.8 mM, some PB nanocubes formed and dispersed on nitrobenzene-RGO composite surface uniformly (Fig. 2B). The PB nanocube arranged on nitrobenzene-RGO composite surface compactly and formed a monolayer at 1.25 mM (Fig. 2C). The obtained PB nanocubes-nitrobenzene-RGO nanocomposites could be well dispersed in water and ethanol. Further increasing the concentration of FeCl₃–K₃Fe(CN)₆ resulted in some aggregation of PB on nitrobenzene-RGO composite surface as shown in Fig. 2D. The results indicated that the concentration of FeCl₃–K₃Fe(CN)₆ might play a crucial role in PB crystal formation. Although the preparation is time-consuming as compared with electrodeposition [35,41,51], the PB-nanocube monolayers on nitrobenzene-RGO composites could be obtained by slow reaction. However, the multilayers of PB with irregular shape on an electrode surface could be obtained

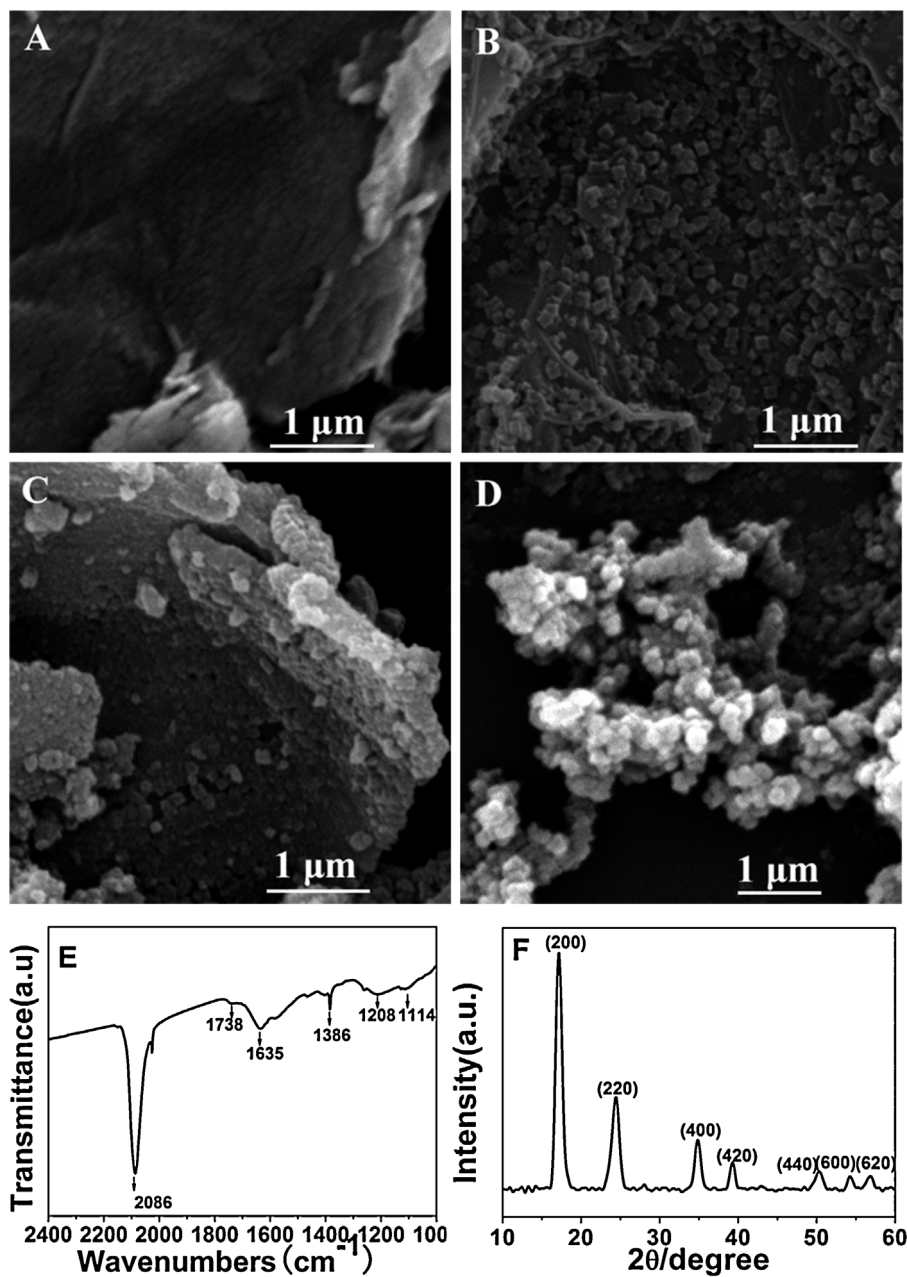


Fig. 2. SEM images of PB nanocubes-nitrobenzene-RGO nanocomposites obtained at different concentration of FeCl₃-K₃Fe(CN)₆: 0.4 (A), 0.8 (B), 1.25 (C) and 1.70 (D) mM. Nitrobenzene-RGO: 0.5 mg mL⁻¹; c_{FeCl₃} / c_{K₃Fe(CN)₆} = 1 : 1. Reaction time: 3 h. FTIR (E) and XRD (F) of PB nanocubes-nitrobenzene-RGO composites (sample B).

by electrodeposition due to rapid reaction and a large number of PB formations in a short time [35,41,51].

The as-prepared nanocomposites were analyzed by FTIR. A new band at 2086 cm⁻¹ was observed in this spectrum compared with that of nitrobenzene-RGO. This new band could be ascribed to stretching modes of the C≡N group in PB nanocube (Fig. 2E) [32,33], indicating the formation of PB on nitrobenzene-RGO sheet. The formation of PB nanocubes-nitrobenzene-RGO nanocomposites was further confirmed by XRD (Fig. 2F). Peaks located at 17.6°, 24.8°, 35.3°, 39.6°, 43.6°, 50.7°, 54.2° and 57.2° can be indexed to the (2 0 0), (2 2 0), (4 0 0), (4 2 0), (4 2 2), (4 4 0), (6 0 0) and (6 2 0) planes of a pure face-centered-cubic Fe^{III}₄[Fe^{II}(CN)₆]₃ (JCPDS card number: 73-0687), respectively (Fig. 2F) [31], demonstrating well crystallized PB nanocubes on the nitrobenzene-RGO composites.

The growth process of PB nanocubes-nitrobenzene-RGO nanocomposites as a function of reaction time was followed by

SEM (Fig. 3). It was obvious that the nitrobenzene-RGO composites still exhibited as sheets with folds (Fig. 3A) [31]. At first 0.5 h, only a few PB nanoparticles (NPs) formed and some folds disappeared (Fig. 3B). The disappearance of folds might be ascribed to the formation of Fe^{III}-Fe^{III}(CN)₆³⁻ complex on nitrobenzene-RGO composites. As the reaction time increased to 1.0 h, more PB NPs were produced and some of them grew into nanocube (Fig. 3C). After 5.0 h, some PB NPs began to inosculate and formed a compacted monolayer as shown in Fig. 3D.

3.3. Electrochemical behaviors of the PB nanocubes-nitrobenzene-RGO nanocomposites/GCE

The electrochemical behaviors of PB nanocubes-nitrobenzene-RGO nanocomposites/GCE were investigated by cyclic voltammograms (CVs). Fig. 4A shows the CVs of PB

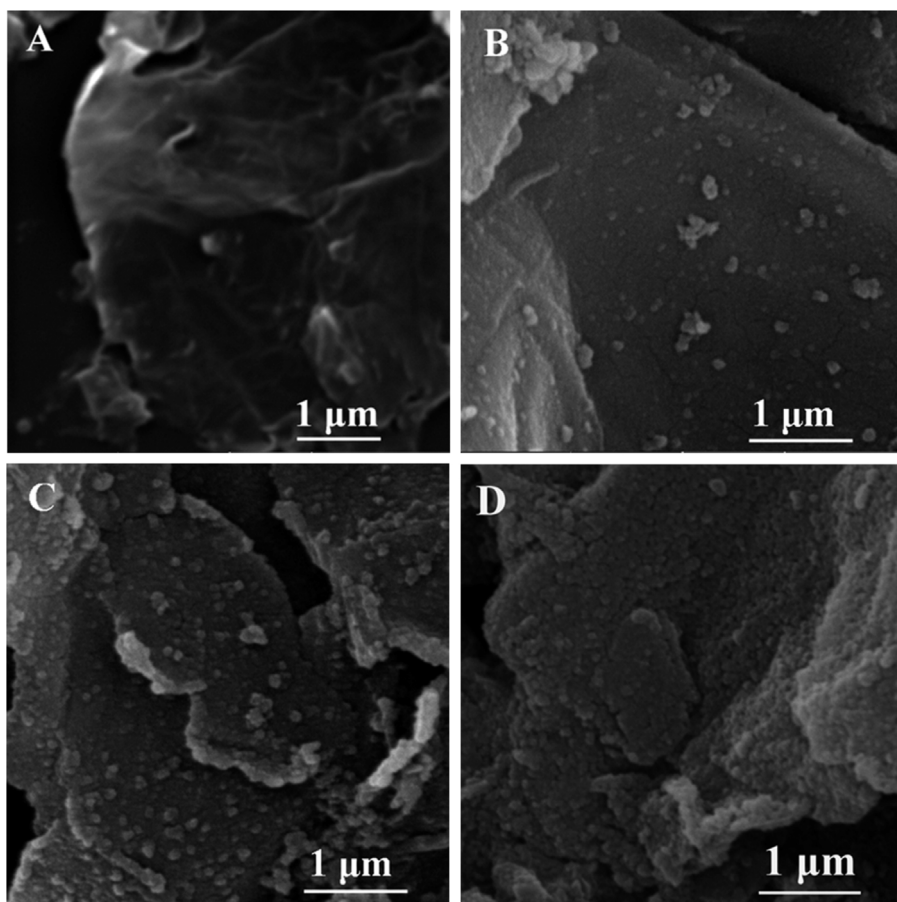
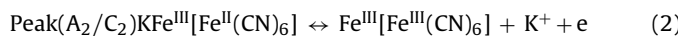
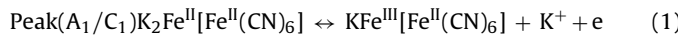


Fig. 3. SEM images of PB nanocubes-nitrobenzene-RGO nanocomposites obtained at different reaction time: 0 (A), 0.5 (B), 1.0 (C) and 5.0 (D) h. Nitrobenzene-RGO: 0.5 mg mL⁻¹; $c_{\text{FeCl}_3 + \text{K}_3\text{Fe}(\text{CN})_6} = 0.8$ mM; $c_{\text{FeCl}_3}/c_{\text{K}_3\text{Fe}(\text{CN})_6} = 1 : 1$.

nanocubes-nitrobenzene-RGO nanocomposites/GCE in 0.05 M PBS + 0.1 M KCl (pH 6.0). The CVs exhibited two anodic peaks at 0.25 V (A_1) and 0.95 V (A_2), respectively. On the reverse scan, the corresponding cathodic peaks C_1 and C_2 appeared at 0.15 V and 0.84 V, respectively. The corresponding $E_{1/2}$ ($E_{1/2} = 1/2(E_{pa} + E_{pc})$) for the two redox transitions A_1/C_1 and A_2/C_2 were 100 and 110 mV, respectively. When the freshly deposited $\text{Fe}^{\text{III}}_4[\text{Fe}^{\text{II}}(\text{CN})_6]_3$ was cycled in a solution containing K^+ in the potential range from -0.4 to 1.2 V, the $\text{Fe}^{\text{III}}_4[\text{Fe}^{\text{II}}(\text{CN})_6]_3$ was transformed to the $\text{KFe}^{\text{III}}[\text{Fe}^{\text{II}}(\text{CN})_6]$ [53]. According to previous results [34,35], the first redox (A_1/C_1) was ascribed to the transitions between PB ($\text{KFe}^{\text{III}}[\text{Fe}^{\text{II}}(\text{CN})_6]$) and Prussian white ($\text{K}_2\text{Fe}^{\text{II}}[\text{Fe}^{\text{II}}(\text{CN})_6]$, PW) and the second redox (A_2/C_2) was attributed to the transitions between PB and Berlin green ($\text{Fe}^{\text{III}}[\text{Fe}^{\text{III}}(\text{CN})_6]$, BG). The two couples of redox peaks in the CVs might be represented by the following reactions [34]:



To further understand the electrochemical behaviors of PB nanocubes-nitrobenzene-RGO nanocomposites/GCE, we paid more attention to the redox transitions A_1/C_1 . Fig. 4B shows the CVs of PB nanocubes-nitrobenzene-RGO nanocomposites/GCE at different scan rate range from 10 to 400 mV s⁻¹. In the potential range of -0.2–0.8 V, the peak current grew as the scan rate increased. The peak current was proportional to the square root of scan rate as shown by the inset in Fig. 4B, indicating that the electron transfer reaction involved a diffusion-controlled process. As mentioned

above, the redox process of PB nanocubes was accompanied with the transfer of K^+ . Thus, the slow diffusion of K^+ might control the electrochemical process and result in the linear dependence of the peak current on the square root of scan rate. The surface average concentrations of electro-active PB nanocubes (Γ^* , mol cm⁻²) could be estimated by Faraday's law [52]:

$$I_p = \frac{nFQv}{4RT} = \frac{n^2F^2A\Gamma^*v}{4RT} \quad (3)$$

which can come to the expression as follows:

$$\Gamma^* = \frac{Q}{nFA} \quad (4)$$

where Γ^* is surface coverage of the redox species and v is the potential scan rate, A is the electrode surface geometrical area, n represents the number of electrons involved in reaction and other symbols have their usual meaning. The calculated value of Γ^* was about 2.11×10^{-8} mol cm⁻² for PB nanocubes-nitrobenzene-RGO nanocomposites/GCE, larger than some electrodeposited PB film electrodes (6.90×10^{-10} mol cm⁻²) [53].

CVs were also performed to evaluate the stability of PB nanocubes layer to pH and temperature changes. Fig. 5A and B shows CVs of PB nanocubes-nitrobenzene-RGO nanocomposites/GCE between -0.2 and +0.6 V (scan rate 50 mV s⁻¹) in buffer solution at pH 3 and pH 7, respectively. The good stability of PB nanocubes layer can even be observed at pH 7, which is superior to previous results [31–35]. Compared with PB-GO (Fig. 5C), the PB nanocubes-nitrobenzene-RGO nanocomposites showed good stability. Fig. 5D shows the CVs of PB nanocubes-nitrobenzene-RGO nanocomposites/GCE at different temperature. It is obvious that

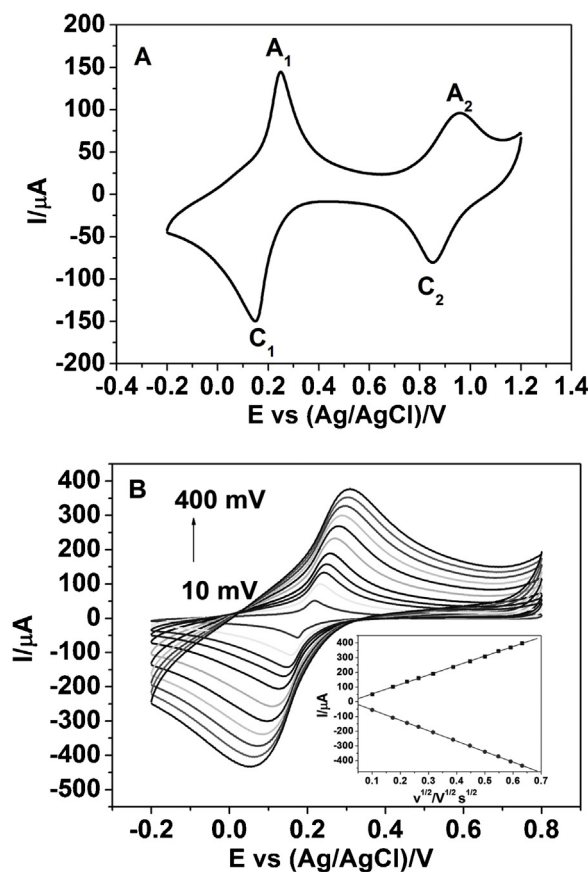


Fig. 4. (A) Cyclic voltammograms (CVs) of PB nanocubes-nitrobenzene-RGO nanocomposites/GCE in 0.05 M PBS + 0.1 M KCl (pH 6.0) at the potential of −0.2–1.2 V. (B) CVs of PB nanocubes-nitrobenzene-RGO nanocomposites/GCE in 0.05 M PBS + 0.1 M KCl solution (pH 6.0) at various scan rates: 10, 30, 50, 70, 100, 150, 200, 250, 300, 350, 400 mV s^{−1} (from inner to outer), respectively. Inset: plot of peak currents versus the square root of scan rates. PB nanocubes-nitrobenzene-RGO nanocomposites/GCE was constructed by casting 6 μL 2 mg mL^{−1} PB nanocubes-nitrobenzene-RGO nanocomposites (sample B in Fig. 2) on GCE.

the PB nanocubes layer is very stable at high temperature. Furthermore, the electron transfer was enhanced as temperature increased due to fast mass transport. The good stability might result from the electrostatic interactions and coordination interaction between Fe³⁺ and nitro-groups on nitrobenzene-RGO composites. The PB nanocubes-nitrobenzene-RGO nanocomposites show good stability under critical operating conditions just owing to the strong

interaction between the PB nanocubes and the nitrobenzene-RGO composites. However, the PB on an electrode surface obtained by electrodeposition showed a weak interaction with electrode surface and might become unstable under oscillation and stirring, regardless of stability under pH [54,55].

3.4. Electrocatalytic reduction of H₂O₂ on PB nanocubes-nitrobenzene-RGO nanocomposites/GCE

The sensing application of PB nanocubes-nitrobenzene-RGO nanocomposites/GCE toward H₂O₂ was investigated. To assess the effect of nitrobenzene on the electrocatalytic reduction of H₂O₂, the electrocatalytic reduction of H₂O₂ at PB nanocubes-nitrobenzene-RGO nanocomposites/GCE and PB-RGO/GCE was compared as shown in Fig. 6A. It obviously indicated that the electrocatalytic reduction peak current at the PB nanocubes-nitrobenzene-RGO nanocomposites/GCE was much larger than that of PB-RGO/GCE, suggesting the nitrobenzene did play an important role in the electrocatalytic reduction of H₂O₂ because it resulted in the large number of PB nanocubes with nanoscaled dimension. Fig. 6B showed the CVs of PB nanocubes-nitrobenzene-RGO nanocomposites/GCE in 0.05 M PBS + 0.1 M KCl (pH 6.0) in the presence of H₂O₂ (1.0–8.0 mM) at a scan rate of 50 mV s^{−1}. The reduction peak at about 0.14 V increased gradually and the oxidation peak decreased slightly with the increase of H₂O₂, showing a typical electrocatalytic reduction process. Fig. 6C showed plot of catalytic current at PB nanocubes-nitrobenzene-RGO nanocomposites/GCE versus the concentration of FeCl₃–K₃Fe(CN)₆ used to prepare PB nanocubes-nitrobenzene-RGO nanocomposites. It was found that the catalytic current of the sensor strongly depended on the concentration of FeCl₃–K₃Fe(CN)₆ and the protocol using 0.8 mM at 3 h showed the largest catalytic current. Fig. 6D showed the plot of catalytic current in the presence of 3 mM H₂O₂ versus the amount of PB nanocubes-nitrobenzene-RGO nanocomposites casting on GCE. It reveals that the catalytic current of the sensor increased as the amount of PB nanocubes-nitrobenzene-RGO nanocomposites casting on GCE increased at first. After too much PB nanocubes-nitrobenzene-RGO nanocomposites was casted on GCE surface, the catalytic current decreased sharply due to poor electron transfer and compact film of PB nanocubes-nitrobenzene-RGO nanocomposites. The largest catalytic current occurred at 6 μL 2 mg mL^{−1} PB nanocubes-nitrobenzene-RGO nanocomposites.

The amperometric response of PB nanocubes-nitrobenzene-RGO nanocomposites/GCE for successive addition of H₂O₂ was investigated in Fig. 7A (curve a). The reduction current could achieve 95% of the steady-state current within 2 s. The current

Table 1

Comparison of the performance of various H₂O₂ sensors constructed based on PB.

Electrode	Detection limit (μmol L ^{−1})	Linear range (mmol L ^{−1})	Sensitivity (μA cm ^{−2} mM ^{−1})	References
PB-RGO/GCE ^a	0.045	5 × 10 ^{−5} –0.12	nr	[31]
PB-GO/GCE ^b	nr	0.05–140	nr	[32]
PB-RGO/GCE ^c	1.9	0.02–0.2	196.6	[33]
PB/graphite electrode	1.0	2.1 × 10 ^{−3} –0.14	138.6	[34]
PB/GO/GCE ^d	0.122	5 × 10 ^{−3} –1.2	408.7	[35]
PB-chitosan-RGO/GCE ^e	0.213	0.01–0.4	816.4	[40]
PB-RGO/GCE ^f	3.0	0.01–1.44	530.0	[41]
PB-FCNFs/GCE ^g	0.7	4.2 × 10 ^{−3} –25	62.4	[44]
PB-nitrobenzene-RGO/GCE	0.4	1.2 × 10 ^{−3} –15.25	300.16	This work

^a PB-RGO nanosheets was first synthesized and then PB-RGO/GCE was prepared by casting the PB-RGO solution on GCE.

^b PB-GO nanosheets was first synthesized and then PB-GO/GCE was prepared by casting the PB-GO solution on GCE.

^c PB-RGO nanosheets with good dispersibility in aqueous solutions was first synthesized and then PB-RGO/GCE was prepared by casting the PB-RGO solution on GCE followed by Nafion.

^d PB-GO/GCE was prepared by electrodepositing PB on GO modified GCE.

^e PB-chitosan-RGO nanosheets was first synthesized and then PB-chitosan-RGO/GCE was prepared by casting the PB-chitosan-RGO solution on GCE.

^f PB-RGO/GCE was prepared by electrodepositing of PB on RGO modified GCE.

^g PB grows on carboxyl group-functionalized carbon nanofibers/GCE.

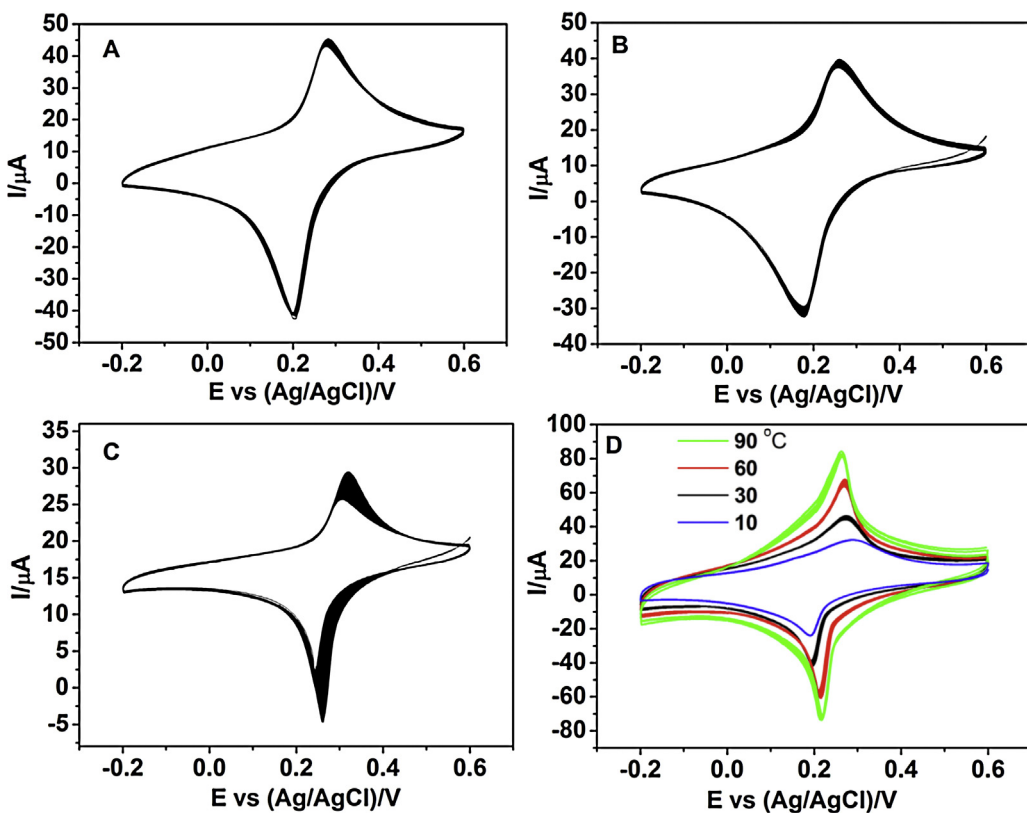


Fig. 5. CVs of PB nanocubes-nitrobenzene-RGO nanocomposites/GCE ((A) and (B)) and PB-GO/GCE (C) in 0.05 M buffer + 0.1 M KCl at pH 3 (A) and pH 7 ((B) and (C)) under 25 °C for 40 cycles. (D) CVs of PB nanocubes-nitrobenzene-RGO nanocomposites/GCE at pH 7 at different temperature for 40 cycles.

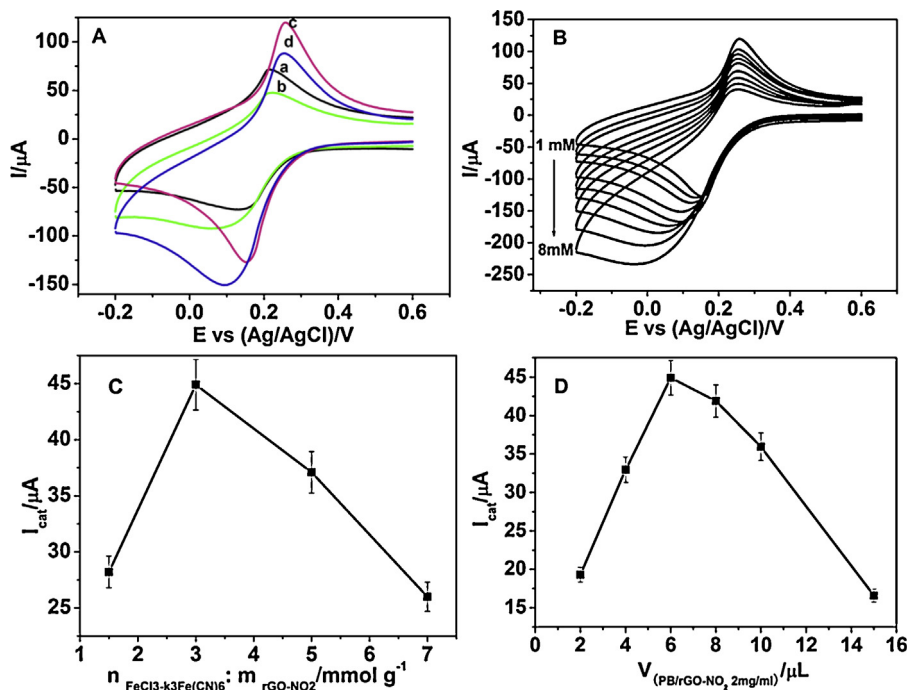


Fig. 6. (A) CVs of PB-RGO/GCE ((a) and (b)), and nitrobenzene-Gr nanocomposites/GCE ((c) and (d)) in 0.05 M PBS + 0.1 M KCl (pH 6.0) in the presence ((b) and (d)) and absence ((a) and (c)) of 3.0 mM H₂O₂ at a scan rate of 50 mV s⁻¹. (B) CVs of PB nanocubes-nitrobenzene-RGO nanocomposites/GCE in 0.05 M PBS + 0.1 M KCl (pH 6.0) in the presence of H₂O₂ (1.0–8.0 mM) at a scan rate of 50 mV s⁻¹. (C) Plot of catalytic current at PB nanocubes-nitrobenzene-RGO nanocomposites/GCE versus different concentration of FeCl₃-K₃Fe(CN)₆ used to prepare PB nanocubes-nitrobenzene-RGO nanocomposites. Electrolyte: 0.05 M PBS + 0.1 M KCl (pH 6.0) in the presence of 3 mM H₂O₂. Nitrobenzene-RGO: 0.5 mg mL⁻¹; c_{FeCl₃}/c_{K₃Fe(CN)₆} = 1 : 1. (D) Plot of catalytic current in the presence of 3 mM H₂O₂ versus volume of PB-nitrobenzene-RGO nanocomposites obtained by reacting 0.5 mg mL⁻¹ nitrobenzene-RGO and 0.8 mM FeCl₃-K₃Fe(CN)₆ for 3 h. c_{PB} nanocubes-nitrobenzene-RGO nanocomposites: 2 mg mL⁻¹.

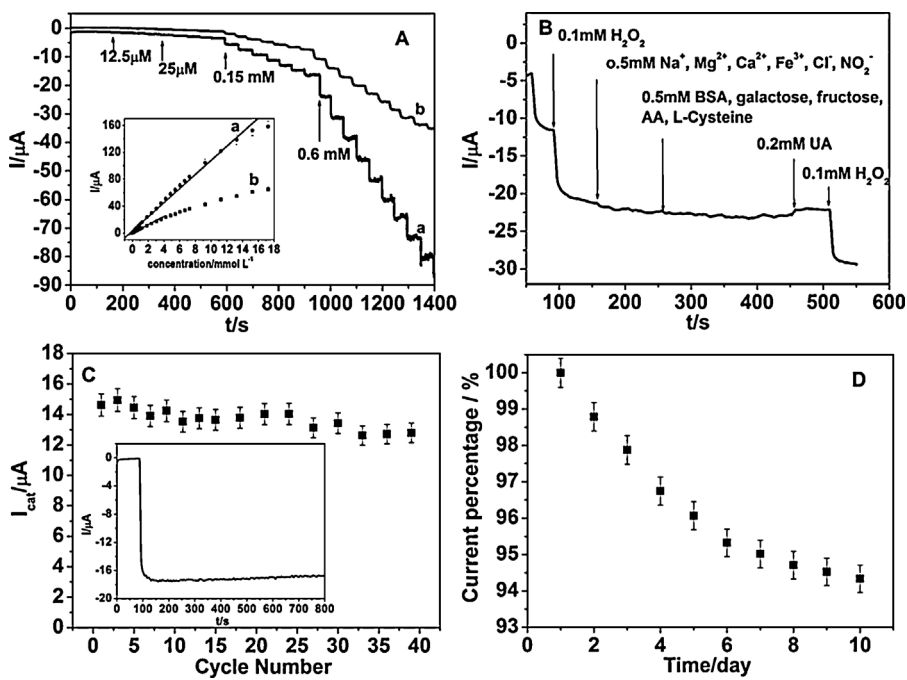


Fig. 7. (A) Typical amperometric response of PB nanocubes-nitrobenzene-RGO nanocomposites/GCE (a) and PB-RGO (b) to successive injection of H₂O₂ into stirred 0.05 M PBS + 0.1 M KCl (pH 6.0) at 0.1 V. Inset: the calibration curve of PB nanocubes-nitrobenzene-RGO nanocomposites/GCE (a) and PB-RGO (b). (B) Interference test of the sensor in 0.05 M PBS + 0.1 M KCl (pH 6.0) in the presence of H₂O₂ and different interference at 0.1 V. (C) Forty-round continuous detection of 1 mM H₂O₂ in 0.05 M PBS + 0.1 M KCl (pH 6.0). Detection method is the same as that described in (A). Inset: The recorded chronoamperogram during long time (10 min). (D) Current response of PB nanocubes-nitrobenzene-RGO nanocomposites/GCE for H₂O₂ over ten days.

response was enhanced as more H₂O₂ was added. Inset (curve *a*) in Fig. 7A showed the calibration curve of the PB nanocubes-nitrobenzene-RGO nanocomposites/GCE. The linear range of the H₂O₂ detection was from 1.2 μM to 15.25 mM ($r=0.994$) with a sensitivity of $300.16 \mu\text{A cm}^{-2} \text{mM}^{-1}$ at 0.1 V. The detection limit was estimated to be 0.4 μM based on the criterion of a signal-to-noise ratio of 3. While the PB-RGO/GCE showed linear range from 2.1×10^{-3} –2.5 mM with a sensitivity of $196 \mu\text{A cm}^{-2} \text{mM}^{-1}$ at 0.1 V (curve *b* in inset in Fig. 7A), which is smaller than that of PB nanocubes-nitrobenzene-RGO/GCE. A comparison of the performance for H₂O₂ sensing of our newly designed sensor to those of other sensors already reported in literature was listed in Table 1. Up to now, many H₂O₂ sensors have been developed based on PB, and all of them have some advantages and limitations [31–35,40,44,53–57]. Taking PB-chitosan-RGO/GCE [40] as an example, the detection limit was pretty low, while the linear range was rather narrow. The H₂O₂ sensors based on electrodeposited PB usually showed a narrow linear range, regardless of low detection limit and high sensitivity. It was noticeable that the detection limit and sensitivity of our sensor was comparable with that of sensor based on electrodeposited PB even or nano-electrode array and ultramicroelectrode [56].

Fig. 7B showed the interference test of the sensor. Chemicals such as bovine serum albumin (BSA), ascorbic acid (AA), galactose, fructose, L-cysteine in a 5-fold concentration, urea acid (UA) in 2-fold concentration and common ions such as Na⁺, Ca²⁺, Mg²⁺ and Fe³⁺ in a 5-fold concentration did not show interference to H₂O₂ detection. To precisely evaluate the run-to-run deviation of H₂O₂ detection, a PB nanocubes-nitrobenzene-RGO nanocomposites/GCE was used to continuously detect 1.0 mM H₂O₂ (in 0.05 M PBS + 0.1 M KCl pH 6.0) for 40 times, only 8% of catalytic current lost after 40 runs of H₂O₂ detection (Fig. 7C). The current response kept 95% of the original value for 0.5 mM H₂O₂ in 10 min in one measurement (inset in Fig. 7C). After the sensor was stored in the inverted beaker at room temperature for 10 days, the current

response to 1.0 mM H₂O₂ only decreased 5.7% of the original current (Fig. 7D). The results reveal that the sensor has very good stability. The electrode-to-electrode repeatability was determined from the response to 1.0 mM H₂O₂ at five different sensors, yielding a RSD of 6.2%.

3.5. Amperometric responses of the GOD/PB nanocubes-nitrobenzene-RGO nanocomposites/GCE toward glucose

Due to its good electrocatalytical activity of PB nanocubes-nitrobenzene-RGO nanocomposites/GCE to the reduction of H₂O₂, the PB nanocubes-nitrobenzene-RGO nanocomposites-based glucose biosensor was further developed. Fig. 8A showed the CVs of GOD/PB nanocubes-nitrobenzene-RGO nanocomposites/GCE in 0.05 M PBS + 0.1 M KCl (pH 6.0) in the presence of glucose (1.0–5.0 mM) at a scan rate of 50 mV s⁻¹. With the increasing of glucose, the catalytic current at GOD/PB nanocubes-nitrobenzene-RGO nanocomposites/GCE increased gradually, exhibiting good electrocatalytic ability toward glucose. Fig. 8B shows the amperometric response of the resulted GOD/PB nanocubes-nitrobenzene-RGO/GCE to glucose in air-saturated stirring 0.05 M PBS + 0.1 M KCl (pH 6.0). The time required for reaching the 95% steady-state response was within 2 s at the biosensor. The Inset I in Fig. 8B showed the calibration curve of the glucose sensor. The linear range of the glucose detection was from 0.016 to 8.5 mM ($r=0.998$) with a slope of $46.7 \mu\text{A cm}^{-2} \text{mM}^{-1}$ at 0 V. The detection limit was estimated to be 5 μM based on the criterion of a signal-to-noise ratio of 3. It is well known that the diabetic glucose concentration is above 6.0 mM, which indicates that the resulted biosensor is suitable for the practical determination of human blood glucose concentration. Human serum samples were made up of many substances, thus interference is inevitable in the determination of glucose. Chemicals such as uric acid, ascorbic acid, galactose, fructose, lactate, BSA and L-cysteine in a 5-fold concentration and common ions

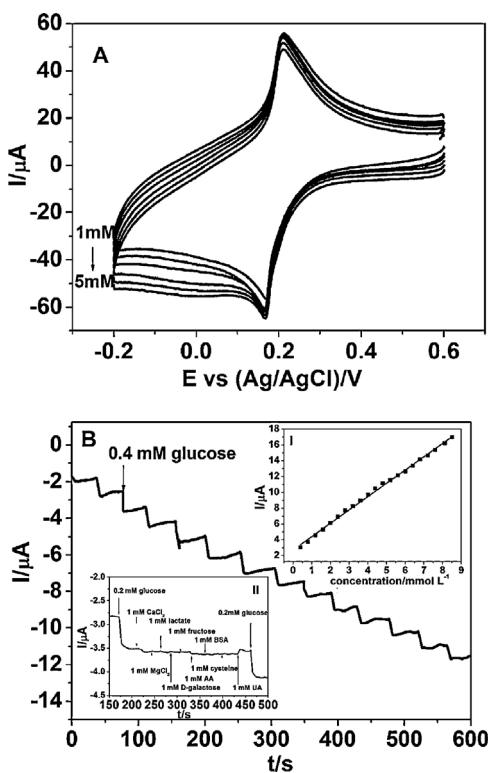


Fig. 8. (A) CVs of GOD/PB nanocubes-nitrobenzene-RGO nanocomposites/GCE in 0.05 M PBS + 0.1 M KCl (pH 6.0) in the presence of glucose (1.0–5.0 mM) at a scan rate of $50 \text{ mV}^{-1} \text{ s}^{-1}$. (B) Typical amperometric response of GOD/PB nanocubes-nitrobenzene-RGO nanocomposites/GCE to successive injection of glucose into stirred 0.05 M PBS + 0.1 M KCl (pH 6.0). Applied potential was 0 V. Inset I: the calibration curve and Inset II: interference test of the sensor in 0.05 M PBS + 0.1 M KCl (pH 6.0) in the presence of glucose and different interference.

such as Ca^{2+} and Mg^{2+} in a 5-fold concentration did not show interference to glucose detection (inset II in Fig. 8B). The stability of the sensor was also investigated. After the sensor was stored in the inverted beaker at 4°C for 30 days, the current response to 1.0 mM glucose only decreased 4.1% of the original current. The repeatability of the current response of one resulted sensor to five successive amperometric measurements of 1.0 mM glucose was checked. A relative standard deviation value (RSD) of 5.2% was calculated for the steady current density. The electrode-to-electrode repeatability was determined from the response to 1.0 mM glucose at five different sensors. They yielded a RSD of 5.6%.

4. Conclusions

In summary, a novel PB nanocubes-nitrobenzene-RGO nanocomposites was prepared. The electrochemical and electrocatalytic behaviors of the PB nanocubes-nitrobenzene-RGO nanocomposites/GCE were explored in detail. Our experiments confirmed that the PB nanocubes-nitrobenzene-RGO nanocomposites/GCE showed good electrocatalytic ability for the reduction of H_2O_2 . As compared to the commercial H_2O_2 sensor, the H_2O_2 sensor based on PB nanocubes-nitrobenzene-RGO nanocomposites has the advantage of good stability and selectivity. Since H_2O_2 is a product from the reduction of O_2 followed by that GOD catalyzes the oxidation of glucose to gluconic acid. Further immobilizing GOD on the PB nanocubes-nitrobenzene-RGO nanocomposites/GCE, an amperometric glucose biosensor was achieved by monitoring the generated H_2O_2 . The resulted glucose biosensor exhibited good performance for glucose detection. Therefore, the proposed sensors might be used as a promising one for practical application.

Acknowledgment

This work was financially supported by National Natural Science Foundation of China (21065005, 21165010 and 21101146), Young Scientist Foundation of Jiangxi Province (20112BCB23006; 20122BCB23011), Foundation of Jiangxi Educational Committee (GJJ13243 and GJJ13244), the State Key Laboratory of Electroanalytical Chemistry (SKLEAC201310), the Open Project Program of Key Laboratory of Functional Small organic molecule, Ministry of Education, Jiangxi Normal University (No. KLFS-KF-201214; KLFS-KF-201218) and Innovation Foundation for graduate student of Jiangxi Province (YC2012-S052) and Jiangxi Normal University (YJS2012090).

References

- [1] W. Chen, S. Cai, Q.Q. Ren, Y.D. Zhao, Recent advances in electrochemical sensing for hydrogen peroxide: a review, *Analyst* 137 (2012) 49.
- [2] Y.H. Song, L. Wang, C.B. Ren, G.Y. Zhu, Z. Li, A novel hydrogen peroxide sensor based on horseradish peroxidase immobilized in DNA films on a gold electrode, *Sens. Actuators, B* 114 (2006) 1001.
- [3] E.C. Hurdis, H. Romeyn, Accuracy of determination of hydrogen peroxide by cerate oxidimetry, *Anal. Chem.* 26 (1954) 320.
- [4] B. Tang, L. Zhang, K. Xu, FIA-near-infrared spectrofluorimetric trace determination of hydrogen peroxide using trichlorobocyanine dye (Cy.7.Cl) and horseradish peroxidase (HRP), *Talanta* 68 (2006) 876.
- [5] H. Wei, E.K. Wang, Fe_3O_4 magnetic nanoparticles as peroxidase mimetics and their applications in H_2O_2 and glucose detection, *Anal. Chem.* 80 (2008) 2250.
- [6] Q. Chang, K. Deng, L. Zhu, G. Jiang, C. Yu, H. Tang, Determination of hydrogen peroxide with the aid of peroxidase-like Fe_3O_4 magnetic nanoparticles as the catalyst, *Microchim. Acta* 165 (2012) 299.
- [7] X.H. Li, Z.J. Zhang, L. Tao, M. Gao, Sensitive and selective chemiluminescence assay for hydrogen peroxide in exhaled breath condensate using nanoparticle-based catalysis, *Spectrochim. Acta, Part A* 107 (2013) 311.
- [8] Y.H. Song, L.L. Wan, Y. Wang, S.C. Zhao, H.Q. Hou, L. Wang, Electron transfer and electrocatalysis of cytochrome c and horseradish peroxidase on DNA modified electrode, *Bioelectrochemistry* 89 (2012) 29.
- [9] L. Bahshi, M. Frasconi, R. Tel-Vered, O. Yehezkel, I. Willner, Following the biocatalytic activities of glucose oxidase by electrochemically cross-linked enzyme-Pt nanoparticles composite electrodes, *Anal. Chem.* 80 (2008) 8253.
- [10] Y.H. Song, K. Cui, L. Wang, S.L. Chen, The electrodeposition of Ag nanoparticles on a type I collagen-modified glassy carbon electrode and their applications as a hydrogen peroxide sensor, *Nanotechnology* 20 (2009) 105501.
- [11] W.P. Lian, L. Wang, Y.H. Song, H.Z. Yuan, S.C. Zhao, P. Li, L.L. Chen, A hydrogen peroxide sensor based on electrochemically roughened silver electrodes, *Electrochim. Acta* 54 (2009) 4334.
- [12] L. Wang, H.Z. Zhu, Y.H. Song, L. Liu, Z.F. He, L.L. Wan, S.L. Chen, P. Xiang, S.S. Chen, J. Chen, Architecture of poly(*o*-phenylenediamine)-Ag nanoparticle composites for a hydrogen peroxide sensor, *Electrochim. Acta* 60 (2012) 314.
- [13] L.L. Wan, Y.H. Song, H.Z. Zhu, Y. Wang, L. Wang, Electron transfer of co-immobilized cytochrome c and horseradish peroxidase in chitosan-graphene oxide modified electrode, *Int. J. Electrochem. Sci.* 6 (2011) 4700.
- [14] C.L. Guo, Y.H. Song, H. Wei, P.C. Li, L. Wang, L.L. Sun, Y.J. Sun, Z. Li, Room temperature ionic liquid doped DNA network immobilized horseradish peroxidase biosensor for amperometric determination of hydrogen peroxide, *Anal. Bioanal. Chem.* 389 (2007) 527.
- [15] J.B. Jia, B.Q. Wang, A.G. Wu, G.J. Cheng, Z. Li, S.J. Dong, A method to construct a third-generation horseradish peroxidase biosensor: self-assembling gold nanoparticles to three-dimensional sol-gel network, *Anal. Chem.* 74 (2002) 2217.
- [16] Y.H. Song, Y. Wang, H.Y. Liu, L. Wang, A novel tri-protein bio-interphase composed of cytochrome c, horseradish peroxidase and concanavalin A: electron transfer and electrocatalysis, *Int. J. Electrochem. Sci.* 7 (2012) 11206.
- [17] Y.H. Song, Y. Wang, L. Wang, H.Y. Liu, Electron transfer and electrocatalysis of layer-by-layer (DNA/Cyt c-HRP)n multilayer, *Int. J. Electrochem. Sci.* 7 (2012) 9375.
- [18] X. Li, Q. Zhu, S. Tong, W. Wang, W. Song, Self-assembled microstructure of carbon nanotubes for enzymeless glucose sensor, *Sens. Actuators, B* 136 (2009) 444.
- [19] L.Z. Gao, J. Zhuang, L. Nie, J.B. Zhang, Y. Zhang, N. Gu, T.H. Wang, J. Feng, S. Yang, D.L. Perrett, X.Y. Yan, Intrinsic peroxidase-like activity of ferromagnetic nanoparticles, *Nature Nanotech.* 2 (2007) 577.
- [20] X.X. Liu, H. Zhu, X.R. Yang, An amperometric hydrogen peroxide chemical sensor based on graphene- Fe_3O_4 multilayer films modified ITO electrode, *Talanta* 87 (2011) 243.
- [21] Z.X. Zhang, H. Zhu, X.L. Wang, X.L. Wang, X.P. Yang, Sensitive electrochemical sensor for hydrogen peroxide using Fe_3O_4 magnetic nanoparticles as a mimic for peroxidase, *Microchim. Acta* 17 (2011) 183.
- [22] H. Cui, W. Wang, C.F. Duan, Y.P. Dong, J.Z. Guo, Synthesis, characterization, and electrochemiluminescence of luminol-reduced gold nanoparticles and their application in a hydrogen peroxide sensor, *Chem. Eur. J.* 13 (2007) 6975.

- [23] W.B. Lu, F. Liao, Y.L. Luo, G.H. Chang, X.P. Sun, Hydrothermal synthesis of well-stable silver nanoparticles and their application for enzymeless hydrogen peroxide detection, *Electrochim. Acta* 56 (2011) 2295.
- [24] K. Cui, Y.H. Song, Y. Yao, Z.Z. Huang, L. Wang, A novel hydrogen peroxide sensor based on Ag nanoparticles electrodeposited on DNA-networks modified glassy carbon electrode, *Electrochim. Commun.* 10 (2008) 663.
- [25] S. Liu, J.Q. Tian, L. Wang, X.P. Sun, A method for the production of reduced graphene oxide using benzylamine as a reducing and stabilizing agent and its subsequent decoration with Ag nanoparticles for enzymeless hydrogen peroxide detection, *Carbon* 49 (2011) 3158.
- [26] J.S. Huang, D.W. Wang, H.Q. Hou, T.Y. You, Electrospun palladium nanoparticle-loaded carbon nanofibers and their electrocatalytic activities towards hydrogen peroxide and NADH, *Adv. Funct. Mater.* 18 (2008) 441.
- [27] Y. Liu, D.W. Wang, L. Xu, H.Q. Hou, Y.Y. You, A novel and simple route to prepare a Pt nanoparticle-loaded carbon nanofiber electrode for hydrogen peroxide sensing, *Biosens. Bioelectron.* 26 (2011) 4585.
- [28] T. Niazov, B. Shlyahovsky, L. Willner, Photoswitchable electrocatalysis and catalyzed chemiluminescence using photoisomerizable monolayer-functionalized surfaces and Pt nanoparticles, *J. Am. Chem. Soc.* 129 (2007) 6374.
- [29] M. Riskin, R. Tel-Vered, I. Willner, Thermo-switchable charge transport and electrocatalysis using metal-ion-modified pNIPAM-functionalized electrodes, *Adv. Funct. Mater.* 19 (2009) 2474.
- [30] F.G. Xu, M. Deng, G.Y. Li, S.L. Chen, L. Wang, Electrochemical behavior of cuprous oxide-reduced graphene oxide nanocomposites and their application in nonenzymatic hydrogen peroxide sensing, *Electrochim. Acta* 88 (2013) 59.
- [31] L. Cao, Y. Liu, B. Zhang, L. Lu, In situ controllable growth of prussian blue nanocubes on reduced graphene oxide: facile synthesis and their application as enhanced nanoelectrocatalyst for H_2O_2 reduction, *ACS Appl. Mater. Interfaces* 2 (2010) 2339.
- [32] X.W. Liu, Z.J. Yao, Y.F. Wang, X.W. Wei, Graphene oxide sheet-Prussian blue nanocomposites: green synthesis and their extraordinary electrochemical properties, *Colloids Surf., B* 81 (2010) 508.
- [33] E. Jin, X.F. Lu, L.L. Cui, D.M. Chao, C. Wang, Fabrication of graphene/Prussian blue composite nanosheets and their electrocatalytic reduction of H_2O_2 , *Electrochim. Acta* 55 (2010) 7230.
- [34] B. Haghghi, H. Hamidi, L. Gorton, Electrochemical behavior and application of Prussian blue nanoparticle modified graphite electrode, *Sens. Actuators, B* 147 (2010) 270.
- [35] Y. Zhang, X. Sun, L. Zhu, H. Shen, N. Jia, Electrochemical sensing based on graphene oxide/Prussian blue hybrid film modified electrode, *Electrochim. Acta* 56 (2011) 1239.
- [36] K.S. Novoselov, A.K. Geim, S.V. Morozov, D. Jiang, Y. Zhang, S.V. Dubonos, I.V. Grigorieva, A.A. Firov, Electric field effect in atomically thin carbon films, *Science* 306 (2004) 666.
- [37] A.K. Geim, K.S. Novoselov, The rise of graphene, *Nat. Mater.* 6 (2007) 183.
- [38] J.C. Meyer, A.K. Geim, M.I. Katsnelson, K.S. Novoselov, T.J. Booth, S. Roth, The structure of suspended graphene sheets, *Nature* 446 (2007) 60.
- [39] D. Chen, H.B. Feng, J.H. Li, Graphene oxide: preparation, functionalization, and electrochemical applications, *Chem. Rev.* 112 (2012) 6027.
- [40] J.H. Yang, N. Myoung, H.G. Hong, Facile and controllable synthesis of Prussian blue on chitosan-functionalized graphene nanosheets for the electrochemical detection of hydrogen peroxide, *Electrochim. Acta* 81 (2012) 37.
- [41] Y.Y. Jiang, X.D. Zhang, C.S. Shan, S.C. Hua, Q.X. Zhang, X.X. Bai, L. Dan, L. Niu, Functionalization of graphene with electrodeposited Prussian blue towards amperometric sensing application, *Talanta* 85 (2011) 76.
- [42] W. Hummers, R. Offeman, Preparation of graphitic oxide, *J. Am. Chem. Soc.* 80 (1958) 1339.
- [43] E. Belyarova, M.E. Itkis, P. Ramesh, C. Berger, M. Sprinkle, W.A. de Heer, R.C. Haddon, Chemical modification of epitaxial graphene: spontaneous grafting of aryl groups, *J. Am. Chem. Soc.* 131 (2009) 1336.
- [44] L. Wang, Y.J. Ye, H.Z. Zhu, Y.H. Song, S.J. He, F.G. Xu, H.Q. Hou, Controllable growth of Prussian blue nanostructures on carboxylic group-functionalized carbon nanofibers and its application for glucose biosensing, *Nanotechnology* 23 (2012) 455502.
- [45] J.W. An, Y.C. Zhou, H.F. Zhao, Y.X. Ma, M.L. Li, S.M. Li, Polyaniline-grafted graphene hybrid with amide groups and its use in supercapacitors, *J. Phys. Chem. C* 116 (2012) 19699.
- [46] X. Chen, S.Q. Liu, Y.H. Song, S.J. Dong, Fabrication and characterization of ordered oligoaniline film, *Chem. Lett.* 31 (2002) 552.
- [47] C.S. Shan, H.F. Yang, D.X. Han, Q.X. Zhang, A. Ivaska, L. Niu, Graphene/AuNPs/chitosan nanocomposites film for glucose biosensing, *Biosens. Bioelectron.* 25 (2010) 1070.
- [48] Y.H. Song, Y.Q. Liu, M.L. Yang, B.L. Zhang, Z. Li, Diluting thiol-derivatized oligonucleotide monolayers on Au(111) by mercaptohexanol replacement reaction, *Appl. Surf. Sci.* 252 (2006) 5693.
- [49] W. Zhang, L.L. Wang, N. Zhang, G. Wang, B. Fang, Functionalization of single-walled carbon nanotubes with cubic Prussian blue and its application for amperometric sensing, *Electroanalysis* 21 (2009) 2325.
- [50] J.F. Zhai, Y.M. Zhai, D. Wen, S.J. Dong, Prussian blue/multiwalled carbon nanotube hybrids: synthesis, assembly and electrochemical behavior, *Electroanalysis* 21 (2009) 2207.
- [51] P. Salazar, M. Martín, R.D. O'Neill, R. Roche, J.L. González-Mora, Improvement and characterization of surfactant-modified Prussian blue screen-printed carbon electrodes for selective H_2O_2 detection at low applied potentials, *J. Electroanal. Chem.* 675 (2012) 48.
- [52] A.J. Bard, L.R. Faulkner, *Electrochemical methods: fundamentals and applications*, second ed., John Wiley and Sons, Inc, New York, 2001.
- [53] J.J. García-Jareño, J.N. Avarro-Laboulais, F. Vicente, Electrochemical study of nafion membranes/Prussian blue films on ITO electrodes, *Electrochim. Acta* 4 (1996) 2675.
- [54] D. Moscone, D. D'Ottavi, D. Compagnone, G. Palleschi, Construction and analytical characterization of Prussian blue-based carbon paste electrodes and their assembly as oxidase enzyme sensors, *Anal. Chem.* 73 (2001) 2529.
- [55] F. Ricci, A. Amine, G. Palleschi, D. Moscone, Prussian Blue based screen printed biosensors with improved characteristics of long-term lifetime and pH stability, *Biosens. Bioelectron.* 18 (2003) 165.
- [56] A.A. Karyakin, E.A. Kuritsyna, E.E. Karyakina, V.L. Sukhanov, Diffusion controlled analytical performances of hydrogen peroxide sensors: towards the sensor with the largest dynamic range, *Electrochim. Acta* 54 (2009) 5048.
- [57] F. Ricci, A. Amine, C.S. Tuta, A.A. Ciucu, F. Lucarelli, G. Palleschi, D. Moscone, Prussian blue and enzyme bulk-modified screen-printed electrodes for hydrogen peroxide and glucose determination with improved storage and operational stability, *Anal. Chim. Acta* 485 (2003) 111.